OUKA
Osaka University Knowledge Archive

Title	Molecular dynamics simulation of the formation of sp3 hybridized bonds in hydrogenated diamondlike carbon deposition processes
Author(s)	Murakami, Yasuo; Horiguchi, Seishi; Hamaguchi, Satoshi
Citation	Physical Review E - Statistical, Nonlinear, and Soft Matter Physics. 81(4) p.041602
Issue Date	2010-04-05
oaire:version	VoR
URL	https://hdl.handle.net/11094/78474
rights	Copyright (2010) by the American Physical Society
Note	

Osaka University Knowledge Archive : OUKA

https://ir.library.osaka-u.ac.jp/

Osaka University

Molecular dynamics simulation of the formation of sp^3 hybridized bonds in hydrogenated diamondlike carbon deposition processes

Yasuo Murakami,[1] Seishi Horiguchi,[2] and Satoshi Hamaguchi[1,*]
[1]*Center for Atomic and Molecular Technologies, Osaka University, 2-1 Yamadaoka, Suita, Osaka 565-0871, Japan*
[2]*Canon ANELVA Corporation, 2-5-1 Kurigi, Asao-ku, Kawasaki, Kanagawa 215-8550, Japan*
(Received 15 October 2009; published 5 April 2010)

The formation process of sp^3 hybridized carbon networks (i.e., diamondlike structures) in hydrogenated diamondlike carbon (DLC) films has been studied with the use of molecular-dynamics simulations. The processes simulated in this study are injections of hydrocarbon (CH_3 and CH) beams into amorphous carbon (a-C) substrates. It has been shown that diamondlike sp^3 structures are formed predominantly at a subsurface level when the beam energy is relatively high, as in the "subplantation" process for hydrogen-free DLC deposition. However, for hydrogenated DLC deposition, the presence of abundant hydrogen at subsurface levels, together with thermal spikes caused by energetic ion injections, substantially enhances the formation of carbon-to-carbon sp^3 bonds. Therefore, the sp^3 bond formation process for hydrogenated DLC films essentially differs from that for hydrogen-free DLC films.

DOI: 10.1103/PhysRevE.81.041602 PACS number(s): 81.15.Aa, 52.77.Dq, 52.40.Hf, 52.65.Yy

I. INTRODUCTION

Amorphous carbon with a high content of sp^3 structures is often called diamondlike carbon (DLC) and known to have extraordinary material properties such as high mechanical hardness, high wear resistance, low friction coefficients, high chemical inertness, good infrared (IR) transparency, high electrical resistivity, good field-emission properties, and low dielectric coefficients [1–7]. Some of these properties have been widely exploited in industrial applications of DLC films. Especially a good combination of high mechanical hardness, high wear resistance, and low friction coefficients makes DLC suitable for use in coating technologies. Furthermore, the heterogeneous growth of DLC films on various materials at low deposition temperatures can be achieved with relative ease by plasma-enhanced chemical vapor deposition (PECVD). In PECVD processes, the material properties can be fine-tuned by a right combination of process parameters. With such favorable properties, DLC is widely used, for example, as protection layers for data storage disks and magnetic recording heads.

Amorphous carbon may be classified into different groups based on the content of hydrogen (H) atoms as well as sp^3 and sp^2 hybridized carbon (C) atoms [2]. Among them, DLC that contains at least some amount of hydrogen is called hydrogenated DLC whereas hydrogen-free DLC is often termed tetrahedral amorphous carbon (ta-C). Sometimes, hydrogenated DLC with a higher content of sp^3 hybridized carbon is termed hydrogenated tetrahedral amorphous carbon (ta-C:H) [7]. For most practical applications, hydrogenated DLC is more widely used than hydrogen-free DLC (i.e., ta-C), so the standard term "DLC" commonly refers to hydrogenated DLC [5].

In the absence of hydrogen, the formation mechanisms of sp^3 hybridized bonds during a carbon deposition process have been extensively discussed [1–7]. The subplantation model, which was proposed by Lifshitz *et al.* [8,9], is now widely accepted as a model for the growth process of hydrogen-free DLC. The term "subplantation" indicates shallow implantation of incident energetic species into a subsurface (i.e., near-surface bulk) region of the substrate. The original subplantation model by Lifshitz *et al.* states [8,9], based on the experimental observations, that the formation of sp^3 hybridized bonds occurs predominantly in the subsurface region where the injected C atoms accumulate rather than on the top surface [10].

After the proposal of the subplantation model by Lifshitz *et al.*, details on how sp^3 hybridized bonds actually form in the subsurface region then became the focus of debate. Various models for sp^3 formation mechanisms were subsequently proposed [11–16]. For example, based on the premise that sp^3 hybridized bonds are preferentially generated at the location of a high local density (and accordingly sp^2 at the location of a low local density), Robertson built a model [15,16] that describes the sp^3 formation process in the subsurface by carbon ion incidence, in which sp^3 hybridized bonds are formed by the increase of local density arising from direct penetration of incident ions or knock-on of surface atoms. The model also includes the relaxation process caused by thermal spikes due to the slowdown of injected ions [17].

While carbon hybridization mechanisms for hydrogen-free DLC (ta-C) have been studied extensively, few systematic studies on carbon hybridization mechanisms have been conducted for hydrogenated DLC. With the addition of hydrogen and/or hydrocarbon as incident species, the surface reactions can be far more complex than those by pure carbon incidence. For example, sticking probabilities and surface loss probabilities of saturated hydrocarbon radicals such as CH_3 on hydrogenated amorphous carbon (a-C:H) surface are known to be extremely small [18–21]. The recent radical-beam experiments [22–26] by Schwarz-Selinger *et al.* and von Keudell *et al.* showed that sticking probabilities can vary significantly (by about 2 orders of magnitude) depending on the simultaneously impinging atomic hydrogen flux. Further-

*hamaguch@ppl.eng.osaka-u.ac.jp

 ©2010 The American Physical Society

more, it has been also shown [26] that, with various combinations of simultaneous fluxes of hydrocarbon radicals, atomic hydrogen, and energetic inert ions of 200 eV, the film growth rate varies greatly from highly efficient deposition to significant surface etching. The formation of sp^3 hybridized bonds in deposited films was, however, not examined by these beam studies.

In the present study, in an attempt to develop highly efficient PECVD processes for high-quality hydrogenated DLC films, we examine sp^3 hybridized bond formation mechanisms in a-C:H deposition processes. Especially of interest are the effects of energetic incidence of hydrocarbon fragment ions such as CH_3^+ and CH^+ on an amorphous carbon (a-C) substrate surface. While we expect something similar to subplantation to occur in the process, the formation mechanism of sp^3 hybridized bonds with ready availability of abundant H atoms can be fundamentally different from that in a pure carbon deposition process. Therefore, the goal of this work is to clarify the role of hydrogen in the formation of diamondlike structures in hydrogenated DLC deposition processes.

As a tool for this study, we use classical molecular-dynamics (MD) simulation by which dynamics of individual atoms may be examined in detail. In this study, we examine the initial phase of carbon film deposition by numerically simulating single-species incidence of CH_3 or CH on an a-C film that is initially hydrogen-free. Although the surface reactions that we consider in this study are far simpler than those of any realistic PECVD systems, a better understanding of individual reaction processes such as those examined here will serve as the basis for a more complete understanding of real PECVD processes.

MD simulations have been used by many authors to study carbon film deposition processes. The first published classical MD simulation study on carbon film deposition processes is probably the one by McKenzie *et al.* [12], where ion-injection induced compressive stress in a thin diamond film was examined. The first MD simulation to emulate the growth process of a carbon film was performed by Kaukonen and Nieminen [27], in which energetic C atoms were used as deposition precursors for a hydrogen-free thin carbon film. Subsequent studies on hydrogen-free carbon deposition processes by various types of MD simulations include those by Marks *et al.* [10,17], Uhlmann and Frauenhaim [28], Kaukonen and Nieminen [29], Jäger and Albe [30], Kohary and Kugler [31], and Li *et al.* [32]. Mechanical properties of a-C films were studied with Monte Carlo simulations by Kelires [33–35].

MD studies on the growth processes of hydrogenated DLC films have been, on the other hand, less extensive. Huang *et al.* [36] studied impact-induced chemisorption of CH_3 and CH_2 on a hydrogenated diamond film using classical MD simulations. Neyts *et al.* examined the deposition mechanisms of various types of hydrocarbon radicals with low kinetic energies incident on diamond or DLC surfaces [37–39]. Zhang *et al.* [40], on the other hand, studied the deposition process of CH_3 and other hydrocarbon radicals and ion fragments on a diamond surface. In a different line of research, Miyagawa *et al.* used dynamical Monte Carlo simulations to model deposition processes of hydrogenated DLC films [41–43]. Salonen *et al.* [44] discussed sputtering processes that might occur during deposition processes of hydrogenated a-C films.

The rest of the paper is arranged in the following manner. We first briefly present our MD simulation scheme in the next section. In Secs. III and IV, we describe simulation results and discuss their implications, first on sticking probabilities and second on the formation of diamondlike sp^3 structures. The conclusions are given in Sec. V.

II. MD SIMULATION

In classical MD simulations, trajectories of all atoms in the system are obtained from the integration of Newton's equation of motion [45–48] and macroscopic physical quantities, such as deposition rates and sputtering yields, may be obtained from proper averaging of corresponding microscopic quantities. Atomic interactions in classical MD simulations are predetermined and the interatomic potential functions used in this study are multibody potential functions (similar to Stillinger-Weber functions with bond-order corrections) given in Ref. [46]. In this set of potential functions, the bond order of a carbon-carbon (CC) bond is determined from the number of other carbon (C) and hydrogen (H) atoms that are present in the neighborhoods of the carbon atoms that form the bond in consideration. For example, if there are three H atoms in each neighborhood of the C atom, the CC bond is a single bond whereas if there are two H atoms in each neighborhood, the CC bond is a double bond. A function that counts the neighboring atoms is built in each interatomic potential function, which typically affects the attractive force of an atom-atom interaction. The set of interatomic potential functions given in Ref. [46] also contains functions for nitrogen (N) atoms but nitrogen was not used in the present work. It has been confirmed that some etching and deposition simulations based on MD simulations with the C and H potential functions given in Ref. [46] typically present results similar to those based on the C and H functions given by Brenner [49].

The model substrate used in the simulation is a hydrogen-free amorphous carbon (a-C) cube with an edge length of about 2 nm. It consists of approximately 800 carbon atoms arranged at random positions in the cube. Its mass density is about 2.0 g/cm^3, which is typical for a-C. The system is then brought to thermal equilibrium at 300 K by MD simulation of canonical ensemble (i.e., with constant temperature and density). After thermalization, the model substrate is found to consist mainly of sp^2 hybridized bonds; the ratio of the number of sp^3 C atoms to that of sp^2 atoms in the model substrate is about 0.4%. The periodic boundary conditions are imposed in the lateral directions so that the α-C cube can represent an infinitely wide flat thin film with a thickness of about 2 nm. In the 0.4-nm-thick bottom layer of the substrate cube, the atoms are set immobile lest the substrate drift downward when it is subject to momentum transfer from incident gas-phase species.

It has been known that CH_3 is the most abundant radical species in methane plasmas that are often used for a-C:H deposition in PECVD processes [50–52]. Methyl ion CH_3^+ is

known to form one of the largest ion fluxes emitted from methane plasmas [51]. Therefore, as mentioned earlier, we select CH_3 as energetic incident species in our simulation study. In addition, we have also selected CH as another incident species for comparison since the difference in hydrogen quantity per incidence between CH_3 and CH may give some insight into the role of hydrogen in the deposition processes.

In this MD study, charge-neutral CH_3 or CH species are injected normally into the top surface of the model substrate with incident energies in the range of from 2 to 50 eV. These are typical kinetic energies of energetic species in PECVD processes [50]. In actual PECVD processes, such energetic species are most likely positive ions accelerated by the bias voltage although some charge-neutral species may also have high kinetic energies because of charge-exchange reactions. In our MD simulation, however, all species, including those with high kinetic energies, are treated as charge neutral, so that all interatomic forces can be modeled by those for charge-neutral species of Ref. [46] for the sake of simplicity.

The sequence of deposition simulations is the following [45–48]. A single simulation cycle starts with an injection of a CH_3 or CH atomic cluster at a predetermined kinetic energy into the substrate surface. The substrate is set in thermal equilibrium at 300 K. The initial lateral position of the injected species is randomly selected and its initial height is set to be about 1 nm above the substrate surface. The incident angle is normal to the substrate surface, as mentioned earlier. The trajectories of all atoms are then obtained from the integration of Newton' equation of motion under the condition of constant total energy, i.e., microcanonical conditions, for 0.8 ps. The numerical time integration is based on the velocity Verlet algorithm. The system is then rapidly cooled and equilibrated at the initial temperature (300 K) during the following 0.2 ps to remove the excess heat from the system. The next simulation cycle then starts with a new particle injection, as in the first cycle. In the MD simulation study presented here, such simulations cycles are typically repeated 800–1000 times, which correspond to the beam dose (i.e., fluence) of 2.0×10^{16}–2.5×10^{16} cm^{-2}.

III. SIMULATION RESULTS: STICKING PROBABILITIES

In this section, we present results of the MD simulation. Shown in Fig. 1 are surface morphologies at a dose of 2.0×10^{16} cm^{-2} of (a) CH_3 and (b) CH incidences at 20 eV on the a-C model substrate. Here, large black spheres represent C atoms in the bottom layer which are assumed to be immobile. The gray spheres represent mobile C atoms that initially constitute the substrate. The large white spheres represent injected C atoms. Injected H atoms are represented by small black spheres. Clearly the deposited film is thicker for CH incidence. As will be shown shortly, under all conditions studied in this work, CH has a higher sticking probability than CH_3.

Figure 2 shows that the depth profiles of atomic species at a dose of 2.0×10^{16} cm^{-2} of CH_3 incidence with incident energies of (a) 20 eV and (b) 50 eV. The profiles of substrate C atoms, deposited C atoms, and deposited H atoms are given by the thick solid, broken, and thin solid curves, respectively. The horizontal axis represents the film thickness measured from the bottom of the model substrate. In this figure, the atomic density at each depth is obtained from the

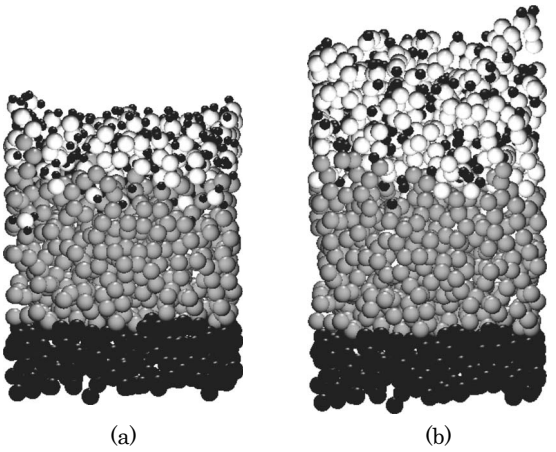

FIG. 1. Surface morphologies after (a) CH_3 and (b) CH incidences obtained from MD simulations. In each case, the beam dose and kinetic energy are 2.0×10^{16} cm^{-2} and 20 eV. The large black and gray spheres represent immobile C atoms in the bottom layer and mobile C atoms of the initial substrate. The large white and small black spheres represent injected C and H atoms.

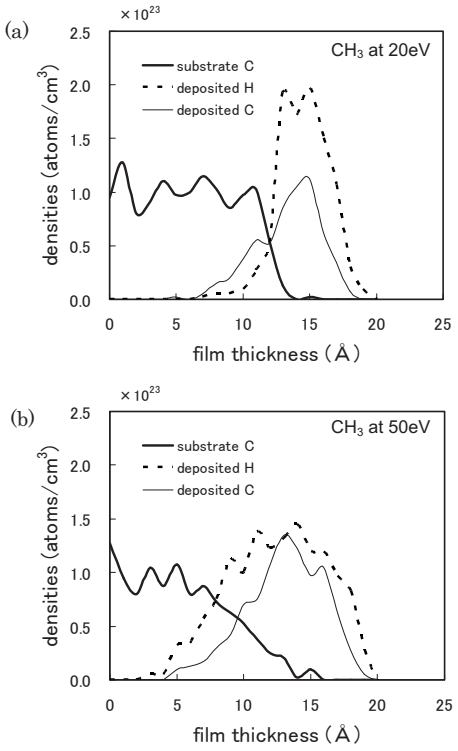

FIG. 2. Depth profiles of atomic species at a dose of 2.0×10^{16} cm^{-2} of CH_3 incidence with incident energies of (a) 20 eV and (b) 50 eV, obtained from MD simulations. The profiles of substrate C atoms, deposited C atoms, and deposited H atoms are given by the thick solid, broken, and thin solid curves, respectively. Horizontal axis represents the film thickness measured from the bottom of the model substrate.

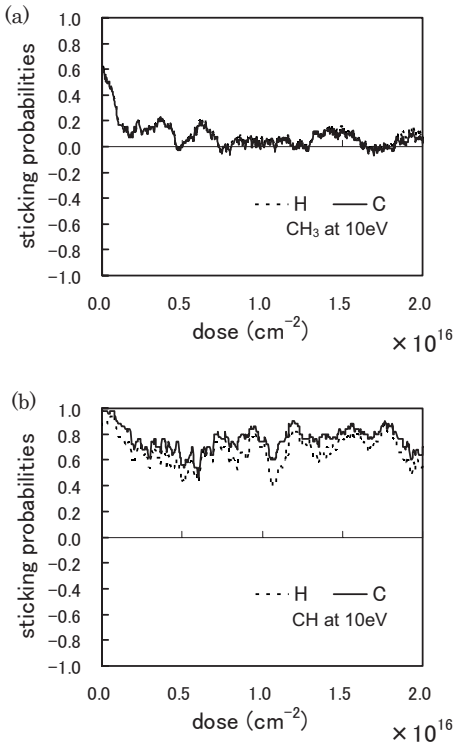

FIG. 3. Sticking probabilities of C and H atoms as functions of the beam dose for (a) CH_3 and (b) CH incidences at 10 eV, obtained from MD simulations.

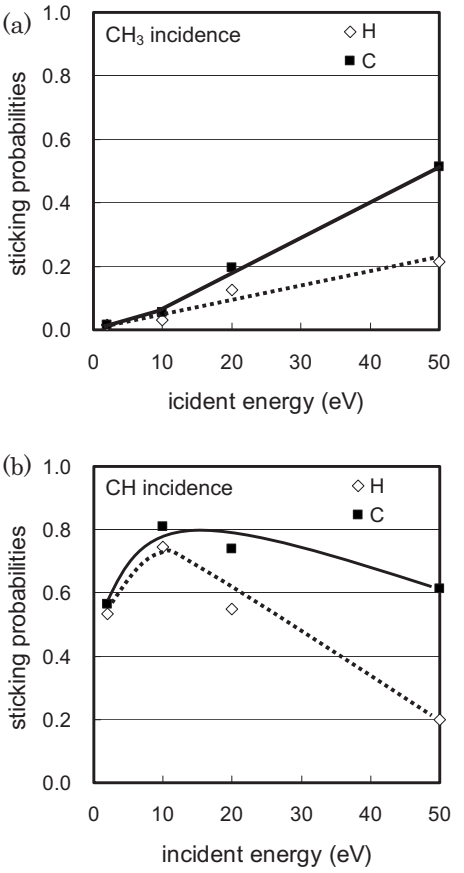

FIG. 4. Sticking probabilities of C (filled squares) and H (empty diamonds) for (a) CH_3 and (b) CH incidences averaged over the beam dose from 1.5×10^{16} to 2.0×10^{16} cm^{-2} as functions of the incident energy, obtained from MD simulations. Solid and dotted curves are guides to the eyes.

total number of the atoms that are present in a 1-Å-thick layer at the depth. The figure clearly shows that deposited C and H atoms penetrate the substrate more deeply at higher energy. Furthermore, H atoms penetrate the substrate more deeply than C atoms because the H atom has a smaller interaction length (i.e., atomic radius) than the C atom.

Figure 3 shows sticking probabilities of C and H atoms as functions of the beam dose for (a) CH_3 and (b) CH incidences at 10 eV. The sticking probability of a C (or H) atom here is defined as the average number of C (or H) atoms that increases in the substrate per injected C (or H) atom when C (or H) atoms are brought to the substrate as part of injected CH_3 or CH atomic clusters. If no substrate atom is removed by the impact of CH_3 or CH (but part of CH_3 or CH may be reflected at the impact), the sticking probability of C (or H) represents literally the probability that the injected C (or H) atom sticks to the substrate surface. On the other hand, if more than one atom is removed from the surface per C (or H) incidence, the sticking probability becomes negative. The sticking probability shown in Fig. 3 is the average over 20 injections (0.5×10^{15} cm^{-2}) around the indicated beam dose. The sticking probabilities of C and H are indicated by the solid and dotted curves in each figure although the both curves nearly coincide and are hardly distinguishable in (a). It is shown in Fig. 3 that the sticking probabilities of both C and H decrease initially and then reach steady state.

The sticking probabilities of C (filled squares) and H (empty diamonds) in steady state are plotted in Fig. 4 as functions of the incident energy for (a) CH_3 and (b) CH incidences. These steady-state values are obtained from the averages over beam dose from 1.5×10^{16} to 2.0×10^{16} cm^{-2}. As expected, when the incident energy is relatively low, the sticking probability for CH incidence is generally higher than that for CH_3. This is because a CH atomic cluster has more dangling bonds than CH_3 and therefore a CH cluster has a higher probability of forming covalent bonds with substrate C atoms.

At higher incident energies, on the other hand, both CH_3 and CH atomic clusters can break into their component atoms upon impact on the surface and their sticking probabilities are more likely to be determined by the number of dangling bonds of C or H rather than the number of dangling bonds of CH_3 or CH atomic clusters. This may make the sticking probabilities for CH_3 and CH incidences take similar values at higher energies (i.e., around 0.6 and 0.2 for C and H at around 50 eV). It is interesting to note that, under the conditions we examine in this work, the sticking probability of C or H from CH_3 impact monotonically increases as a function of the incident energy whereas the sticking probability of C or H from CH impact peaks at around 10 eV. As the probability of substrate atoms being removed (i.e., sputtering yield) typically increases with increasing incident energy, so does the probability of deeper implantation of incident species. Therefore, the peak of sticking probability may appear at some incident energy but no peak of CH_3 sticking probability is observed in the energy range examined there.

In the case of CH_3 beam incidence, if the incident energy is lower than 10 eV, the substrate surface becomes nearly saturated by H atoms supplied by incident CH_3 at an early stage and, after the near saturation, further deposition hardly occurs. In other words, the sticking probability becomes nearly zero in steady state. This result is consistent with earlier experimental studies on this system with CH_3 radical beams [23].

If the incident energy is higher than 10 eV, such H atoms are displaced by incident CH_3 and therefore the sticking probability of C or H increases as a function of the incident energy. As mentioned earlier, the recent radical-beam experiments [22–26] by Schwarz-Selinger *et al.* and von Keudell *et al.* showed that sticking probabilities and film growth rate can vary significantly depending on the impinging hydrogen and hydrocarbon fluxes and kinetic energies of incident beams. These experimental results are consistent with our observation in MD simulations that surface passivation by hydrogen strongly affects the sticking probabilities of incident hydrocarbon species.

It is also shown in Fig. 4 that sticking probability of H is generally lower than that of C, especially at higher energies. At 2 eV, for example, the sticking probabilities of C and H take almost the same values in either (a) or (b), which indicates that the incident clusters, either CH_3 or CH, stick to or are reflected from the surface without breaking up. On the other hand, as the incident energy increases, the difference in the sticking probabilities between C and H increases, which indicates that, at higher energies, C atoms that have more dangling bonds are more easily captured by the substrate surface than H atoms.

IV. SIMULATION RESULTS: FORMATION OF sp^3 HYBRIDIZED BONDS

Hardness of a DLC film is determined by the sp^3 carbon content in the film. In this section, we study how sp^3 hybridized bonds connecting C atoms are formed in the film deposition processes.

The coordination number for a given atom is defined as the number of other atoms that exist in its neighborhood. In the present study, we are interested in the "carbon-to-carbon" (C-to-C) coordination number, which we define as the number of C atoms that exist in the neighborhood of a particular C atom that we consider. For example, in crystalline diamond, the C-to-C coordination number of every C atom is 4. If the C-to-C coordination number of a C atom is 4, then the C atom forms sp^3 hybridized bonds with the surrounding C atoms. Similarly, if the C-to-C coordination number for a C atom is 3, it forms sp^2 hybridized bonds with the surrounding C atoms.

Figure 5 shows the ratio of the number of C atoms with each C-to-C coordination number deposited on the substrate to the number of all deposited C atoms as functions of the incident energy at a dose of 2.5×10^{16} cm^{-2} for (a) CH_3 and (b) CH beam incidences. Especially, the ratio for the C-to-C coordination number being 4 represents the fraction of fully carbon terminated sp^3 C atoms (each of which is bonded with four other C atoms only, not more and not less) for all

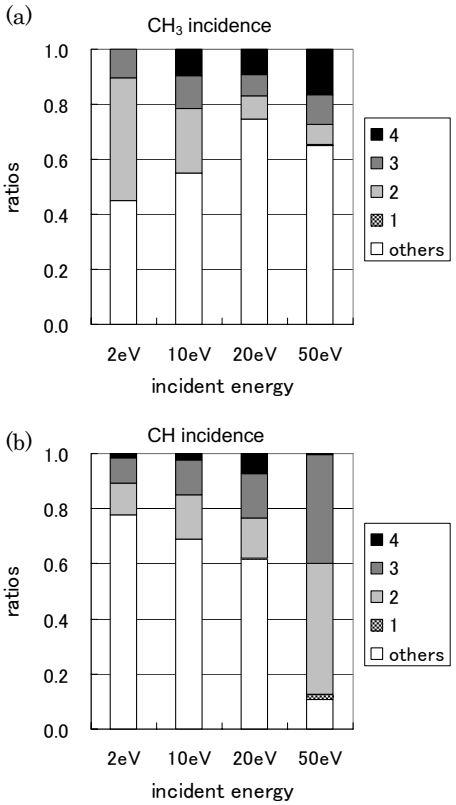

FIG. 5. Ratio of the number of C atoms with each C-to-C coordination number deposited on the substrate to the number of all deposited C atoms as functions of the incident energy at a dose of 2.5×10^{16} cm^{-2} for (a) CH_3 and (b) CH beam incidences, obtained from MD simulations. The "others" include deposited C atoms bonded with one or more H atoms or those bonded with five or more other C atoms (although the latter are scarce).

deposited C atoms. This fraction represents the "diamond-likeness" of the deposited film. Note that C atoms that constitute the initial substrate (which are mostly of sp^2, as mentioned earlier) are not counted in Fig. 5. However, in the C-to-C coordination numbers listed here, bonds connecting deposited C atoms and substrate C atoms are counted. The "others" in Fig. 5 include deposited C atoms bonded with H atoms, possibly together with other neighboring C atoms.

It is clearly seen in Fig. 5 that, for CH_3 incidence, deposited C atoms are more likely to form sp^3 hybridized bonds with other C atoms at higher incident energy under the conditions studied here. A similar tendency is also seen for CH incidence up to 20 eV. However, at 50 eV for CH incidence, the sp^3 fraction is significantly lower, which is likely caused by relative scarcity of hydrogen in the substrate. The sticking coefficient of H atoms for CH incidence is low at high energy, as seen in Fig. 4(b).

Plotted in Fig. 6 are the fully carbon-terminated sp^3 fractions as functions of the CH_3 beam dose at 20 eV (broken curve) and 50 eV (solid curve). As mentioned above, the fully carbon-terminated sp^3 fraction is the same as the ratio denoted by the C-to-C coordination number being 4 in Fig. 5. It is seen that, initially (when the incident-beam dose is lower than about 1.5×10^{16} cm^{-2}), the sp^3 fraction is higher at 20 eV than at 50 eV. It has been observed in our MD

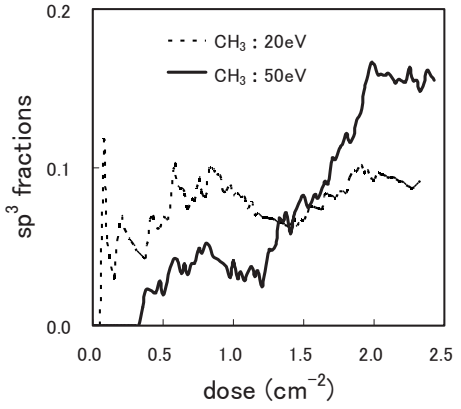

FIG. 6. Fully carbon-terminated sp^3 fractions as functions of the CH_3 beam dose at 20 eV (broken curve) and 50 eV (solid curve), obtained from MD simulations. The fully carbon-terminated sp^3 fraction here is the same as the ratio denoted by the C-to-C coordination number being 4 in Fig. 5 and each C atom counted here is bonded with four other C atoms only.

simulations that incident 20 eV CH_3 species, when they are adsorbed, tend to be adsorbed without breaking up but often displacing H atoms that passivate the substrate surface. An adsorbed CH_3 group with its C atom being bonded with a substrate C atom tends to maintain its sp^3 hybridized (i.e., diamondlike) structure terminated by H atoms on the surface. With a large number of such adsorbed CH_3 groups present on the surface, hydrogen abstraction reactions release hydrogen molecules (H_2) from adjacent CH_3 groups and promote the formation of diamondlike structures on the substrate surface.

At 50 eV incidence, on the other hand, incident CH_3 species tend to break up at impact and the separated C and H atoms typically penetrate the substrate deeply. At a lower beam dose, implanted C atoms tend to form sp^2 bonds with surrounding C atoms in the substrate. However, as the beam dose increases, more and more H atoms that are also accumulated at the subsurface level break up and terminate π bonds and dangling bonds of C atoms there. As more C atoms in the subsurface level have their bonds terminated by H atoms and, furthermore, gain enough mobility from the kinetic energy provided by bombarding incoming species (i.e., thermal spikes [17]), a structural relaxation process takes place more easily. Then, after sufficient desorption of hydrogen molecules from the subsurface level caused by hydrogen abstraction reactions, more carbon-terminated sp^3 hybridized bonds are formed in the subsurface region. In other words, structural relaxation assisted by a high concentration of implanted H atoms and kinetic energy provided by thermal spikes of incident ions help generate more C-to-C sp^3 hybridized bonds at higher dose, as shown in Fig. 6. The kinetic-energy effect mentioned above may be considered as a kind of annealing effects at a microscopic level arising from the thermal spikes.

Figure 7 shows the depth profiles of the (a) C-to-C σ bond density and (b) carbon sp^2 bond density at various beam doses in the case of 50 eV CH_3 beam incidence obtained from MD simulations. Here, the sp^2 bond means a carbon bond that contains a (partial) π orbital, such as the carbon bond of graphite. As in Fig. 2, the horizontal axis in each

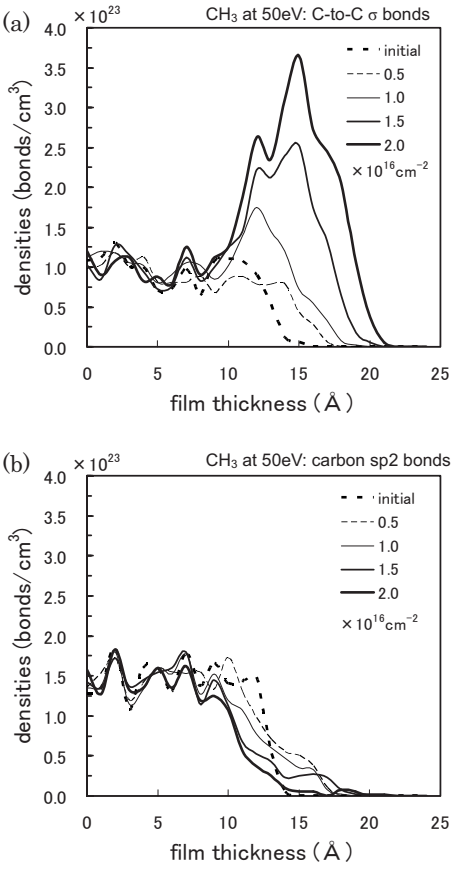

FIG. 7. The depth profiles of the (a) C-to-C σ bond density and (b) carbon sp^2 bond density at various beam doses in the case of 50 eV CH_3 beam incidence, obtained from MD simulations. Here, the sp^2 bond means a carbon bond that contains a (partial) π orbital, such as the carbon bond of graphite. The horizontal axis represents the film thickness measured from the bottom of the model substrate.

figure represents the film thickness measured from the bottom of the model substrate. The bond density at each depth is obtained from the total number of the bonds that are present in a 1-Å-thick layer at the depth. Note that neither C-H nor H-H σ bond is included in Fig. 7(a) [53]. It is seen that, at 50 eV, the number of σ bonds increases as the deposition takes place.

Figure 7(b), on the other hand, shows that the density of sp^2 bonds (many of which existed in the initial substrate) decreases as the beam dose increases. This is due to the increase in atomic hydrogen in the substrate, where H atoms supplied by incident CH_3 break up more π bonds and therefore generate more σ bonds. This process facilitates the structural relaxation of deposited C atoms and the formation of diamondlike carbon structures, as mentioned above.

Figure 8 shows the density profile of fully carbon-terminated sp^3 C atoms at a dose of 2.0×10^{16} cm^{-2} for 50 eV CH_3 incidence (depicted by the gray curve denoted by "sp^3 C"). For reference, the density profiles of C and H atoms are also plotted here, which are the same as those given in Fig. 2(b). Note that "the fully carbon-terminated sp^3 C atom" means a C atom that is bonded with four other C atoms only, as defined in Fig. 5. It is clearly seen that the sp^3

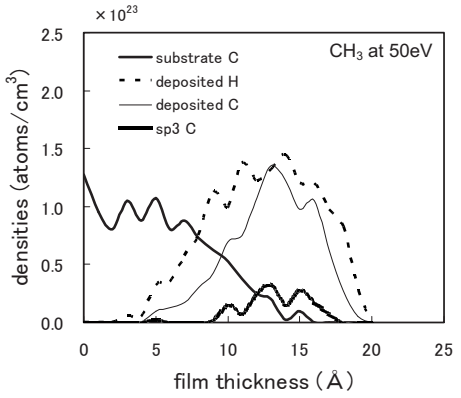

FIG. 8. The depth profile of fully carbon-terminated sp^3 C atoms at a dose of 2.0×10^{16} cm^{-2} for 50 eV CH_3 incidence (depicted by the gray curve denoted by sp^3 C), obtained from MD simulations. For reference, the profiles of C and H atoms are also plotted here, which are the same as those in Fig. 2(b).

C atoms are mostly located in the subsurface level, typically around 1 nm below the top surface in this case.

V. CONCLUSIONS

We have carried out MD simulations to study CH_3 and CH monoenergetic beam deposition processes on a hydrogen-free a-C substrate. First we examined the sticking probabilities of C and H atoms in the processes as functions of beam incident energy and dose. We then examined the structures of deposited films with special attention to the formation of diamondlike structures.

As stated at the outset, the goal of this study is to understand the formation mechanism of diamondlike sp^3 structures in hydrogenated DLC films deposited by, e.g., PECVD processes. We have focused in this study on a relatively early stage of the film deposition process where the deposited film thickness is about 1 nm. The sp^3 carbon content in the deposited film determines the film characteristics. It is typically desired to have a high sp^3 carbon content for high-quality DLC films.

The main conclusion we have drawn in this study is that the sp^3 formation mechanisms are essentially different between hydrogen-free and hydrogenated DLC deposition processes. As we have discussed in the previous section, it is true that, in both hydrogen-free and hydrogenated DLC deposition processes, the sp^3 structures are more efficiently formed at relatively high kinetic energies of incident species. Furthermore, the sp^3 structures are formed predominantly in the subsurface region. Thus the sp^3 formation process in either hydrogen-free or hydrogenated DLC deposition may be called a subplantation process. However, in hydrogenated DLC deposition, the presence of abundant hydrogen at a subsurface level, together with thermal spikes caused by energetic ion incidence, significantly enhances the formation of sp^3 bonds connecting C atoms. This hydrogen-induced formation process of diamondlike structures is so dominant in hydrogenated DLC film deposition that, although it occurs at a subsurface level under the influence of subplantation effects (such as local film densification and induced stress [6,8,9]), it distinguishes itself from a typical sp^3 formation process in hydrogen-free DLC film deposition.

The effect of hydrogen is clearly seen in Fig. 5, where the amount of hydrogen supplied to the substrate is shown to cause significant difference in the formation of diamondlike structures in the deposited films. With more hydrogen readily available in the subsurface level, the fraction of fully carbon-terminated sp^3 bonds is much higher for CH_3 incidence than CH incidence. In this process, abundant hydrogen typically terminates π bonds and dangling bonds of C atoms in the subsurface region and helps to form hydrogen-terminated sp^3 structures first. Then, with the help of thermal spikes arising from energetic ion impact, structural relaxation due to local high "temperature" in the subsurface region promotes hydrogen abstraction reactions by increasing the chance for carbon-terminating H to meet each other in the subsurface region. The increased rate of hydrogen abstraction reactions among carbon-terminating H atoms facilitates the formation of C-C σ bonds.

The importance of the presence of hydrogen is also seen in Fig. 6, which shows that, for 50 eV CH_3 incidence, the fully carbon-terminated sp^3 fraction increases only after sufficient hydrogen implantation takes place. This contrasts well with the sp^3 formation process of hydrogen-free DLC films, in which the diamondlike structures are considered to be formed, in the absence of hydrogen, by local film densification and stress induced by energetic ion bombardment [6,8,9].

We now comment on an issue specific to MD simulations. Our MD simulations (and indeed almost all MD simulations on beam-surface interactions) lack long-time-scale relaxation processes such as surface and solid-phase diffusions. This is because a straightforward implementation of such processes would require prohibitively long computational time and is practically impossible. As mentioned earlier, following a microcanonical simulation of the system for 0.8 ps after each injection of a beam species, the system is cooled to the initial temperature (300 K) within 0.2 ps. Therefore, all particle motions are quenched rapidly (in physical time scales) in our simulations presented here, which prevents any long-time-scale relaxation processes from occurring. During such long-time-scale relaxation processes, sp^3 structures formed upon impact of a beam species may relax to sp^2 structures. On the other hand, it is generally considered that the inverse process, i.e., the further formation of sp^3 structures, hardly takes place during those relaxation processes, especially after the high thermal activation caused by a thermal spike is over. If this conjecture is correct and therefore the majority of experimentally observed diamondlike structures are formed right after each impact of beam species, then the simulation results of this work present, at least qualitatively, physically relevant mechanisms of sp^3 structure formation in hydrogenated DLC film deposition processes.

As to comparison of simulations to experiments, it seems that experimental data on sp^3 structure formation during hydrogenated DLC film deposition by monoenergetic CH_3 or CH beams have been scarce if not nonexistent. Therefore, we have not been able to compare quantitatively the simulation results presented in this paper to corresponding experimental

data. However, several plasma chemical vapor deposition (CVD) and sputter deposition experiments [54–59] have indicated that diamond-likeness of a deposited a-C:H film, such as hardness and content of sp^3 bonds, increases as the bias voltage of the system increases. Such results are consistent with our simulation results given in Fig. 5(a). In the experiments presented in Refs. [54–59], the bias voltage is in the range of a few hundred volts. Because of relatively high pressures often employed in such experiments and also the fact that, in some CH_4 discharges, the $C_2H_5^+$ ion flux is considered to be larger than the CH_3^+ ion flux, the kinetic energy of a single carbon atom in the incident hydrocarbon ion can be much lower than the energy corresponding to the bias voltage. Therefore, the energy range studied in this paper (a few ~50 eV) is not too far from that for typical incident carbon species in actual deposition systems.

ACKNOWLEDGMENTS

The work is partially supported by a Grant-in-Aid for Scientific Research from Ministry of Education, Culture, Sports, Science and Technology (MEXT) Japan. The authors are also grateful for the technical support for computer simulations by M. Isobe of Osaka University, Dr. M. Yamashiro of Nihon University, and K. Hosaka of Canon Inc. and for helpful discussion on DLC experiments with O. Watabe of Canon Anelva Co.

[1] J. Robertson, Surf. Coat. Technol. **50**, 185 (1992).
[2] W. Jacob and W. Möller, Appl. Phys. Lett. **63**, 1771 (1993).
[3] Y. Lifshitz, Diamond Relat. Mater. **5**, 388 (1996).
[4] J. Robertson, Philos. Mag. B **76**, 335 (1997).
[5] A. Grill, Diamond Relat. Mater. **8**, 428 (1999).
[6] J. Robertson, Mater. Sci. Eng. R. **37**, 129 (2002).
[7] C. Casiraghi, A. C. Ferrari, and J. Robertson, Phys. Rev. B **72**, 085401 (2005).
[8] Y. Lifshitz, S. R. Kasi, and J. W. Rabalais, Phys. Rev. Lett. **62**, 1290 (1989).
[9] Y. Lifshitz, S. R. Kasi, and J. W. Rabalais, Phys. Rev. B **41**, 10468 (1990).
[10] N. A. Marks, D. R. McKenzie, and B. A. Pailthorpe, Phys. Rev. B **53**, 4117 (1996).
[11] W. Möller, Appl. Phys. Lett. **59**, 2391 (1991).
[12] D. R. McKenzie, D. Muller, and B. A. Pailthorpe, Phys. Rev. Lett. **67**, 773 (1991).
[13] D. R. McKenzie, J. Vac. Sci. Technol. B **11**, 1928 (1993).
[14] C. A. Davis, Thin Solid Films **226**, 30 (1993).
[15] J. Robertson, Diamond Relat. Mater. **2**, 984 (1993).
[16] J. Robertson, Diamond Relat. Mater. **14**, 942 (2005).
[17] N. A. Marks, Phys. Rev. B **56**, 2441 (1997).
[18] H. Toyoda, H. Kojima, and S. Sugai, Appl. Phys. Lett. **54**, 1507 (1989).
[19] H. Kojima, H. Toyoda, and S. Sugai, Appl. Phys. Lett. **55**, 1292 (1989).
[20] M. Shiratani, J. Jolly, H. Videlot, and J. Perrin, Jpn. J. Appl. Phys., Part 1 **36**, 4752 (1997).
[21] J. Perrin, M. Shiratani, P. Kae-Nune, H. Videlot, J. Jolly, and J. Guillon, J. Vac. Sci. Technol. A **16**, 278 (1998).
[22] T. Schwarz-Selinger, V. Dose, W. Jacob, and A. von Keudell, J. Vac. Sci. Technol. A **19**, 101 (2001).
[23] A. von Keudell, T. Schwarz-Selinger, and W. Jacob, J. Appl. Phys. **89**, 2979 (2001).
[24] A. von Keudell, M. Meier, and T. Schwarz-Selinger, Appl. Phys. A: Mater. Sci. Process. **72**, 551 (2001).
[25] A. von Keudell, M. Meier, and C. Hopf, Diamond Relat. Mater. **11**, 969 (2002).
[26] T. Schwarz-Selinger, M. Meier, C. Hopf, A. von Keudell, and W. Jacob, Vacuum **71**, 361 (2003).
[27] H.-P. Kaukonen and R. M. Nieminen, Phys. Rev. Lett. **68**, 620 (1992).
[28] S. Uhlmann and Th. Frauenheim, Phys. Rev. Lett. **81**, 641 (1998).
[29] M. Kaukonen and R. M. Nieminen, Phys. Rev. B **61**, 2806 (2000).
[30] H. U. Jäger and K. Albe, J. Appl. Phys. **88**, 1129 (2000).
[31] K. Kohary and S. Kugler, Phys. Rev. B **63**, 193404 (2001).
[32] Z. J. Li, Z. Y. Pan, Y. X. Wang, Q. Wei, L. K. Zang, X. S. Ye, T. Bai, C. Wang, and J. R. Liu, Surf. Coat. Technol. **192**, 64 (2005).
[33] P. C. Kelires, Phys. Rev. Lett. **68**, 1854 (1992).
[34] P. C. Kelires, Phys. Rev. B **47**, 1829 (1993).
[35] P. C. Kelires, Phys. Rev. Lett. **73**, 2460 (1994).
[36] Z. Huang, Z. Y. Pan, Y. X. Wang, and A. J. Du, Surf. Coat. Technol. **158-159**, 94 (2002).
[37] E. Neyts, A. Bogaerts, R. Gijbels, J. Benedikta, and M. C. M. van de Sanden, Nucl. Instrum. Methods Phys. Res. B **228**, 315 (2005).
[38] E. Neyts, A. Bogaerts, and M. C. M. van de Sanden, J. Appl. Phys. **99**, 014902 (2006).
[39] E. Neyts, A. Bogarerts, and M. C. M. van de Sanden, J. Phys.: Conf. Ser. **86**, 012020 (2007).
[40] Y. J. Zhang, G. N. Dong, J. H. Mao, and Y. B. Xie, Chin. Sci. Bull. **53**, 1094 (2008).
[41] Y. Miyagawa, S. Nakao, and S. Miyagawa, Surf. Coat. Technol. **128-129**, 85 (2000).
[42] Y. Miyagawa, S. Nakao, M. Ikeyama, and S. Miyagawa, Surf. Coat. Technol. **136**, 122 (2001).
[43] Y. Miyagawa, H. Nakadate, M. Tanaka, and S. Miyagawa, Surf. Coat. Technol. **156**, 87 (2002).
[44] E. Salonen, K. Nordlund, and J. Keinonen, Phys. Rev. B **63**, 195415 (2001).
[45] H. Yamada and S. Hamaguchi, J. Appl. Phys. **96**, 6147 (2004).
[46] H. Yamada and S. Hamaguchi, Plasma Phys. Controlled Fusion **47**, A11 (2005).
[47] M. Yamashiro, H. Yamada, and S. Hamaguchi, J. Appl. Phys. **101**, 046108 (2007).
[48] M. Yamashiro, H. Yamada, and S. Hamaguchi, Jpn. J. Appl. Phys., Part 1 **46**, 1692 (2007).
[49] D. W. Brenner, Phys. Rev. B **42**, 9458 (1990).
[50] N. Mutsukura, S. Inoue, and Y. Machi, J. Appl. Phys. **72**, 43

(1992).
[51] R. Kleber, M. Weiler, S. Krüger, S. Sattel, G. Kunz, K. Jung, and H. Ehrhardt, Diamond Relat. Mater. **2**, 246 (1993).
[52] P. Pecher and W. Jacob, Appl. Phys. Lett. **73**, 31 (1998).
[53] However, it should be noted that C-to-C σ bonds that do not connect the fully carbon-terminated sp^3 C atoms (such as the C-to-C single bond of the structure-CH_2-CH_3) are also counted in Fig. 7(a). This is the reason why the C-to-C σ bond density of Fig. 7(a) is about 1 order of magnitude higher than the sp^3 carbon density (i.e., the density of fully carbon terminated C atoms) given in Fig. 8.
[54] B. André, F. Rossi, and H. Dunlop, Diamond Relat. Mater. **1**, 307 (1992).
[55] T. Tatsuta, K. Tachibana, and S. Tsuji, Jpn. J. Appl. Phys., Part 1 **33**, 6341 (1994).
[56] S. Zhang, X. T. Zeng, H. Xie, and P. Hing, Surf. Coat. Technol. **123**, 256 (2000).
[57] K. Azuma, H. Inaba, K. Tasaka, S. Fujimaki, and H. Shirai, J. Appl. Phys. **39**, 6427 (2000).
[58] N. Paik, Surf. Coat. Technol. **200**, 2170 (2005).
[59] B. G. Choi, J. K. Kim, W. J. Yang, and K. B. Shim, J. Ceram. Proc. Res. **6**, 101 (2005).